Title
Probing growth of metal—organic frameworks with X-ray scattering and vibrational spectroscopy

Journal
Physical Chemistry Chemical Physics, 24(42)

ISSN
0956-5000

Authors
Lu, Wenchao
Zhang, Emily
Qian, Jin
et al.

Publication Date
2022-11-02

DOI
10.1039/d2cp04375k

Probing Growth of Metal–Organic Frameworks with X-Ray Scattering and Vibrational Spectroscopy

Wenchao Lu,[1] Emily Zhang,[1,2] Jin Qian,[1] Chaya Weeraratna,[1] Megan N. Jackson, [2] Chenhui Zhu,[4] Jeffrey R. Long, [2,3,5] and Musahid Ahmed.[1,]*

[1] Chemical Sciences Division, Lawrence Berkeley National Laboratory, Berkeley, CA 94720, USA

[2] Department of Chemistry, University of California, Berkeley, CA 94720, USA

[3] Material Sciences Division, Lawrence Berkeley National Laboratory, Berkeley, CA 94720, USA

[4] Advanced Light Source, Lawrence Berkeley National Laboratory, Berkeley, CA 94720, USA

[5]Department of Chemical and Biomolecular Engineering, University of California, Berkeley, Berkeley, California 94720, United States

Abstract

Nucleation and crystallization arising from liquid to solid phase are involved in a multitude of processes in fields ranging from materials science to biology. Controlling the thermodynamics and kinetics of growth is advantageous to help tune the formation of complex morphologies. Here, we harness wide-angle X-ray scattering and vibrational spectroscopy to elucidate the mechanism for crystallization and growth of the metal–organic framework Co-MOF-74 within microscopic volumes enclosed in a capillary and an attenuated total reflection microchip reactor. The experiments reveal molecular and structural details of the growth processes, while the results of plane wave density functional calculations allow identification of lattice and linker modes in the formed crystals. Synthesis of the metal-organic framework with microscopic volumes leads to monodisperse, micron-sized crystals, in contrast to those typically observed under bulk reaction conditions. Reduction in the volume of reagents within the microchip reactor was found to accelerate the reaction rate. The coupling of spectroscopy with scattering to probe reactions in microscopic volumes promises to be a useful tool in the synthetic chemist's tool kit to understand the bonding information and has potential in designing complex materials.

1 Introduction

To decarbonize our energy sources and mitigate climate change, we need to design revolutionary new ways of generating, storing and transporting energy.[1] This will require harnessing the vast machinery of synthesis science to design and build new materials.[2] Metal–organic frameworks (MOFs) are becoming increasingly attractive for gas storage,[3] molecular separations,[4] energy storage,[5] catalysis,[6] drug delivery,[7] and chemical sensing[8] due to their chemical tunability and high internal surface area. These crystalline materials are comprised of metal ions connected by organic linkers to form porous structures that can be optimized for a particular purpose, promising a world of molecular-level "crystal engineering."[6] While almost 100,000 MOFs have been synthesized to date,[7] there is little understanding of the synthetic principles behind MOF formation, and instead new MOF syntheses generally rely on brute force strategies such as high-throughput screening and trial-and-error.[8]

Achieving new MOF structures by design requires a mechanistic understanding of how molecular precursors nucleate and grow to form the crystalline materials. These processes in metastable materials like MOFs particularly were mostly driven by kinetics, *i.e.,* the selectivity and yield are dictated by the reaction pathway instead of the free energy of the product. Active kinetic control of emergent behavior in chemical transformations promises revolutionary approaches to targeted synthesis, but will require detailed understanding of reaction-diffusion kinetics on the system-relevant length and time scales, which both span many orders of magnitude. The complexities associated with measuring solution-phase nucleation and growth pathways also necessitate the development of an experimental strategy[9] coupled with computational approaches that span the nanoscale and early timescales of nucleation in solution to form solid-phase MOFs.[2, 10] Furthermore, broadly understanding the mechanisms of liquid-to-solid phase transitions is challenging and new methods that provide real-time feedback on how a synthetic change impacts the reaction mechanism and rate would be extremely valuable in the development of such materials.

The process of crystallization includes a multitude of steps such as forming monomers and a bulk crystal lattice, and the rates for nucleation and growth are greatly affected by the lability of the metal ion.[9, 11-13] We have chosen to study the nucleation and growth of Co-MOF-74, which is also known as CPO-27-Co or Co_2(dobdc) (dobdc^{4-} = 2,5-dioxido-1,4-benzenedicarboxylate), a system that has been studied under bulk reaction conditions.[14, 15] (Figure 1)

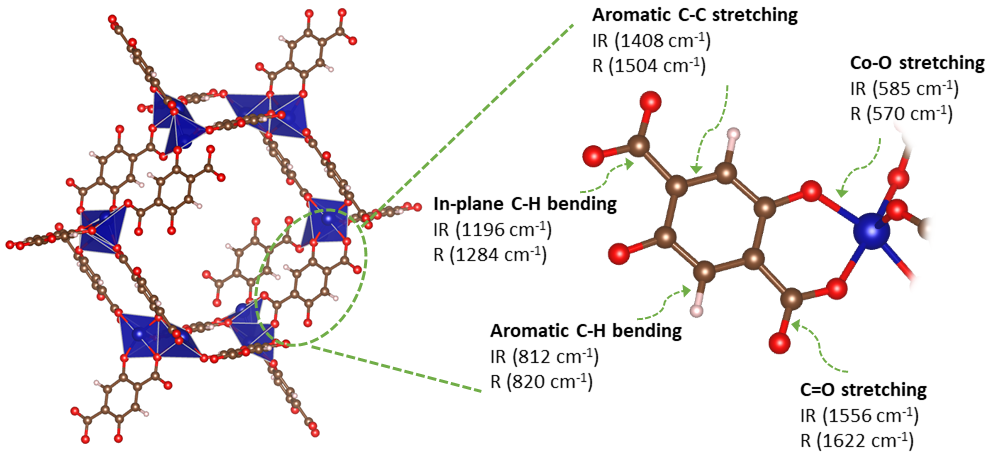

Figure 1 A molecular representation of the Co_2(dobdc). The red balls represent oxygen atoms, brown for carbon atoms, pale pink for hydrogen atoms, and blue for cobalt atoms. Also shown are the linker molecule and the relevant vibrational modes for Raman and Infrared spectroscopy.

Co-MOF-74 is typically synthesized starting with 2,5-dioxido-1,4-benzenedicarboxylic acid and a salt of the octahedral hexaaquo complex of cobalt(II), $[Co(H_2O)_6]^{2+}$. Based on X-Ray diffraction studies, the crystal structure of Co-MOF-74 was revealed to be one-dimensionally arranged honeycomb-like pores with the diameter of 1.1 to 1.2 nm.[16] As crystallization occurs, the crystals elongate along a one-dimensional axis. A series of studies of Co-MOF-74 nucleation and growth showed that the method of heating[14] (ultrasound, microwave and conventional) and mechanochemical synthesis[17] can affect the rate and mechanism of growth for this particular MOF. Hence, the mechanisms of MOF crystallization and the thermodynamic factors that lead to particular kinetics remain elusive, making it challenging to correlate MOF growth across all of the necessary length scales spanning from precursor molecules to crystal.[18, 19]

In this study, we used wide-angle X-ray scattering (WAXS), Raman spectroscopy, mid-infrared (MIR) spectroscopy, and far-infrared (FIR) spectroscopy to investigate the growth kinetics of Co-MOF-74 across various length scales using microscopic volumes of reagents confined either in a capillary or a chip-based reactor. WAXS and FIR spectroscopy provide details about the atomic coordinates and lattice of the MOF, while Raman and MIR spectroscopy provide molecular information on the linker modes. Plane wave density functional theory is used to calculate Raman, FIR, and MIR spectra, to assign modes to the experimental spectra, and to provide a molecular structural view of the MOF. The growth curves of nucleation extracted from the scattering and spectroscopy measurements are compared to earlier reports in the literature. Lowering the reagent volume led to an acceleration of the reaction, suggesting that probing MOF growth in confined reaction geometries is a promising way to explore material growth processes in a controlled environment. We anticipate that the experimental platform can be applied towards rigorous kinetics studies on other framework systems such as covalent organic networks,[20] and zeolites[21] to provide the critical crystal growth and phase change information within the applicable timescale. A clear elucidation of how inorganic crystals nucleate and grow from solution with chemical specificity at relevant time and size domains will be the key to boosting the rational design and synthesis of new frameworks with improved properties.

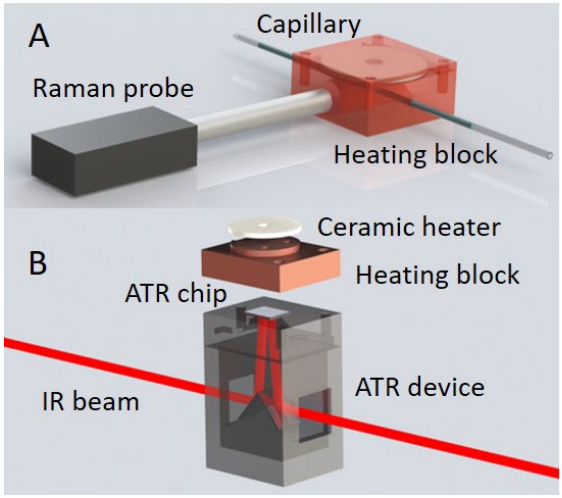

Figure 2 (A) Setup used for Raman and X-Ray scattering. (B) Attenuated Total Reflection (ATR) device for Far and Mid Infrared Spectroscopy.

2 Experimental and Computational

2.1 Wide-Angle X-Ray Scattering.

Wide-angle X-ray Scattering (WAXS) experiments were conducted at Beamline 7.3.3 of the Advanced Light Source, Lawrence Berkeley National Laboratory. Using 10 keV monochromatic X-rays, the beam size was around 300 µm (H) × 700 µm (W), and the distance from the capillary to the detector was calibrated using a silver behenate standard. All raw data were processed using the Nika package29 in Igor Pro 6.37 to produce spectra of Q-vector to intensity. The sample cell consisted of a thin-walled quartz capillary (1.5

mm O.D., Charles Supper Company) connected to syringe pumps enclosed in a copper block that can be heated up to 200 °C with a ceramic heater (Thor Labs). (Figure 2A) After injecting the capillary with Co-MOF-74, it was placed horizontally in front of the X-ray beam shutter to be exposed for 10 seconds in each measurement for reaction time up to 50 minutes and to be captured on camera.

2.2 Raman Spectroscopy.

A Coherent Verdi-V5 laser at 532 nm, was used to perform Raman spectroscopy. The beam was designed to reflect off a 45° broadband dielectric mirror then a 45° long pass dichroic mirror with a 550 nm cutoff to fully reflect green light (532 nm) and transmit red-shifted light (> 550 nm). The collimated light was then focused by an aspheric condenser lens (focal length: 16 mm) to a point 5 mm outside of the lens tube on to the same capillary reactor used for the WAXS measurements. (Figure 2B) Light scattered back towards the lens was collimated, sent back to the dichroic mirror, and captured. A notch filter was used to remove remaining traces of 532 nm light, then a spherical lens was used to focus the beam into a 400 μm optic fiber to a QEPro Spectrometer (Ocean Optics). Spectra of Co-MOF-74 was collected at temperatures ranging from 25°C to 90°C. To calibrate the temperature of the capillary within the heater block, we performed Raman measurements on liquid water in the same geometry and heater conditions. The results are shown in Figure S1 of Supporting Information, and calibrated against literature values of the OH stretch region which acts as an exact thermometer.[22]

2.3 Mid and Far Infrared Spectroscopy.

A Bruker VERTEX70 FT-IR spectrometer equipped with a IRUBIS silicon attenuated total reflection (ATR) chip was used to obtain spectra in the mid- and far-infrared ranges. The cobalt acetate solution in water 3.5 μM and H_4dobdc solution in ethanol 1.0 μM were mixed in a 1:1 ratio, and 200 uL of the mixture was added to the single-bounce ATR chip on a copper block with an inner angle of incidence of 26.7°. A well-shaped cover was then sealed by a 9 mm O.D. x 7 mm I.D. O-ring on the ATR chip to prevent evaporation. The spectra were scanned in the range of 600–4500 cm^{-1}, with a resolution of 4 cm^{-1}, averaged every 64 scans, and corrected using the OMNIC software package (Thermo Scientific). The reactor was calibrated using the OH stretch region by comparing spectra of pure water measured using the same device.[23]

2.4 X-Ray Diffraction and Scanning Electron Microscopy

Samples were prepared for imaging by scanning electron microscopy (SEM) by dispersing MOF particles in methanol with a pipette and drop-casting the MOF onto 5 x 5 mm silicon wafer chips (Ted Pella, Inc. Prod. No. 16008). Samples were sputter-coated with ~5 nm Au/Pd alloy prior to imaging to reduce sample charging. Images were collected using an FEI Quanta Dual Beam FIB 0.5–30kV microscope operating at 10 keV at the Biomolecular Nanotechnology Center at UC Berkeley.

The X-ray diffraction pattern was collected using a Rigaku Miniflex Benchtop diffraction instrument in the UC Berkeley, College of Chemistry X-ray Crystallography Facility.

2.5 Ab-initio Simulations

All calculations were performed using periodic plane-wave DFT code with the PBE exchange-correlation functional[24] at generalized gradient approximation (GGA) level, as implemented in Vienna Ab Initio Simulation Package (VASP).[25] The primitive rhombohedral unit cell containing 54 atoms was used for all

calculations with a cutoff energy of 520 eV, and a Monkhorst–Pack k-mesh with 2 × 2 × 2 k-points. Optimized structure has been validated and was obtained from references.[26, 27] The optimized unit cell size is 15.29 Å with R-3 space group, and the formula for the optimized cell is $C_{24}H_6O_{18}Co_6$ for Co-MOF-74. The vibrational frequencies and the corresponding IR, Raman intensities of the optimized structures were obtained using density functional perturbation theory (DFPT)[28, 29] through evaluations of Born effective charge tensor and the dynamical matrix at the gamma point. Pre- and post-processing of the calculated spectra were done using Phonopy.[30]

3 Results and Discussion

3.1 Synthesis and Characterization of Co-MOF-74

Co-MOF-74 was synthesized by combining equal volumes of a cobalt acetate solution in water and an H_4dobdc solution in ethanol. The reaction typically leads to crystal formation within a few hours at room temperature and within a few minutes at higher temperatures. To confirm that the reaction being performed in a small volume quartz capillary and ATR chip leads to Co-MOF-74 in the same form prepared under bulk conditions, we performed PXRD and SEM measurements of the microcrystals that appeared in these reactors.

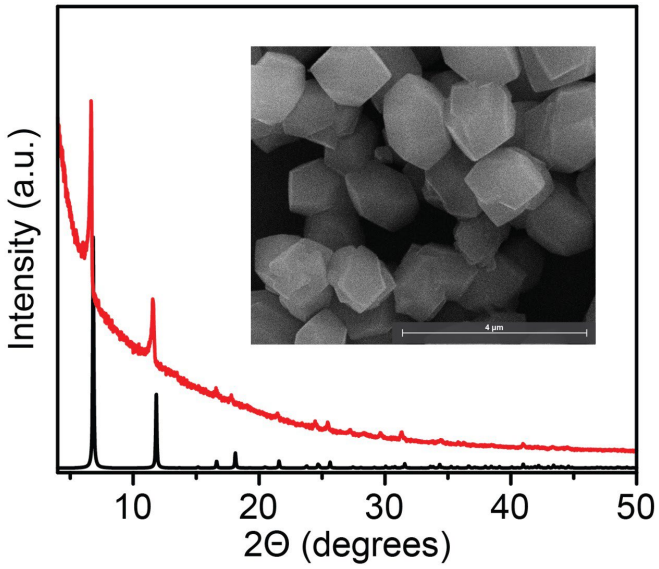

Figure 3 Powder X-ray diffractogram (PXRD) of Co-MOF-74 synthesized on the ATR chip (red) and simulated PXRD of Co-MOF-74 (black). The inset shows a Scanning electron microscopy image of Co_2-(dobdc) of the same sample.

Figure 3 shows a PXRD pattern of the MOF microcrystals synthesized on the chip, which matches the simulated PXRD pattern well. Our results are also in agreement with literature values.[15] The SEM image of the crystals formed on the ATR chip shown in the inset of Figure 3 suggests that they are uniform in size and typically around 2 μm in length in the long dimension.

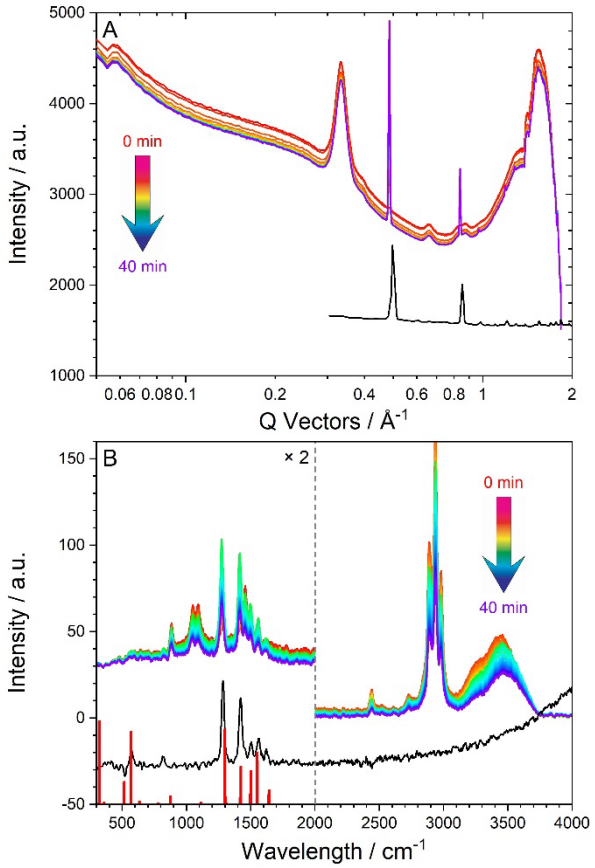

Figure 4 (A) WAXS data as a function of time, collected from a quartz capillary reactor at a heater temperature of 70 °C. The black spectrum is a WAXS pattern from literature[15] collected from a sample of Co-MOF-74. (B) Raman spectra collected from a quartz capillary at a heater temperature of 70 °C. The black spectrum is from MOF crystals formed as a thin film on the inner walls of the capillary after the solvent has been evaporated. The stick figure is a theoretical analysis (blues shifted by 90 cm^{-1}) (to higher frequencies) of the Raman spectrum using plane wave density functional theory.

The initial experiments probing MOF nucleation and growth leveraged WAXS at the Advanced Light Source with temperatures ranging between room temperature and 70 °C. The results at 70 °C are shown in Figure 4A. The first data point collection was at 2 min continuing up to 50 min. Two very sharp peaks positioned at 0.485 and 0.839 $Å^{-1}$ emerge in the WAXS spectra as the reaction progresses towards completion, indicating the formation of a crystal lattice of interatomic distances of 12.96 and 7.49 Å. It is interesting to note that the pore size within the Co-MOF-74 crystal lattice is ~12 Å. [31, 32] These peaks match results obtained for Co-MOF-74 from the literature, which are shown as an inset in the figure.[15] The sharp peaks are the only peaks that increase over time, whereas the rest of the broad scattered background emerging from the reagents decreases over time. There are several other tiny peaks corresponding to shorter interatomic distances, which are difficult to trace their kinetics. Due to the open nature of the capillary, presumably solvent evaporation occurs over time, leading to a decrease in scattering intensity. In our WAXS measurements, the solvent is a 1:1 mixture (by volume) of water and ethanol, and even the highest reaction temperature, 70°C, is still below the boiling point of ethanol. However, at this temperature some solvent evaporation occurred, as we noticed the volume slightly shrunk after 50 minutes of reaction time. This is also confirmed by the baseline lowering of the WAXS spectra."

Next, to obtain molecular information on the crystallization of Co-MOF-74, we coupled the capillary reactor to a home-made Raman spectrometer. The results for 70 °C are shown in Figure 4B. The red spectra mark the beginning of reaction and dark blue the completion of the reaction at 50 min. The results are clear with solvent peaks dominating beyond 1700 cm^{-1}. To disentangle the MOF signal from solvent and reagent, samples which were run at 70° C were left in a fume hood for 24 hours, which led to complete evaporation of solvent. The Raman signal of the residual MOF showed that there was no reagent left in the capillary. A Raman spectrum of the residual MOF that formed as a thin film on the inside of the capillary is shown in black in Figure 4B. We then compared these spectra to literature and DFT calculations performed here, shown as red stick figures in Figure 4B.

The identification is thus (see Figure 1): 570 cm^{-1} (Co-O stretching), 820 cm^{-1} (aromatic C-H bending), 1284 cm^{-1} (in plane C-H bending), 1504 cm^{-1} (aromatic C-C backbone stretching), and 1622 cm^{-1} (C=O stretching) are modes associated with MOF formation, while the peaks in the range 2700-3700 cm^{-1} arise from solvents (ethanol and water). The original kinetics experiment was performed using a Raman assembly which has very low sensitivity below 800 cm^{-1}, while the pure MOF was measured using a new arrangement, hence the Co-O stretching signal can be discerned easily in the solvent free sample.

While the WAXS and Raman spectra from the capillary reactor provided useful structural and molecular information, the time dependence was not satisfactory to extract quantitative kinetics information. This is because the radiation from the Raman laser sometimes caused local heating leading to cavitation and sudden boiling of the solvents within the capillary, followed by the recoil within the capillary from the center, even when we sealed both ends of the capillary. Therefore, our WAXS and Raman experiments herein aim to propose a micro-reactor for qualitatively exploring nucleation, and show its potential for tracing kinetics, and provide structural information on the MOF crystal. To extract reliable mechanistic information and more accurate kinetic parameters for this reaction, we turned to a chip-based FT-ATR FIR and MIR spectroscopic method that we are developing. The volume component of both the capillary and chip-based reactors are similar, 100 and 200 µL respectively. The FIR measurements are complementary to the X-Ray scattering data, since they are sensitive to the lattice of the formed MOF, while the Raman signal is complementary to both FIR and MIR data sets in providing molecular functional group information of the formed MOF.

3.2 Far Infrared and Mid Infrared Spectroscopy and Kinetics of MOF Growth.

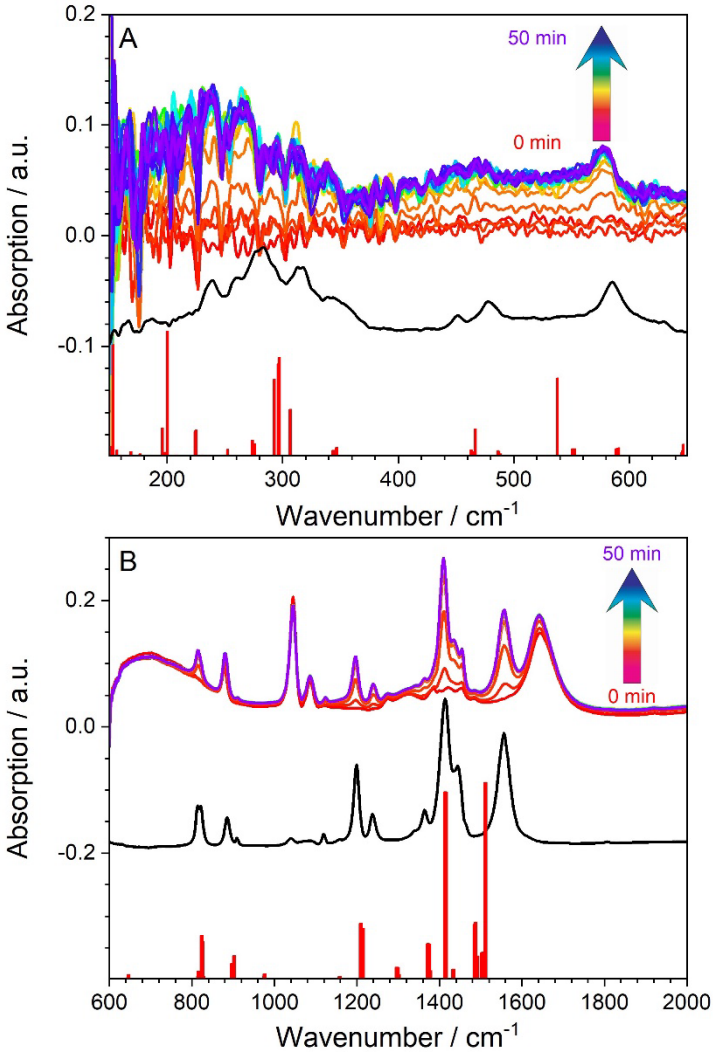

Figure 5 ATR-FIR (A) and (B) ATR-MIR time-dependent data collected from a chip-based reactor at a heater temperature of 70 °C. The black spectrum is from MOF crystals formed on the chip after all solvent has been evaporated off, while the red sticks are from a plane wave density functional calculation scaled by a factor of 1.1.

Figure 5A shows the FIR time traces recorded for the MOF growth at 70 °C. At earlier times (red spectra), the signal is fairly flat, and then increases rapidly to converge to an asymptote (blue spectra). Using a similar procedure performed for the Raman capillary measurement, we removed the solvent by heating the reactor, and the MOF FIR spectrum is shown as a black curve in the figure. Also shown are the stick spectra calculated using plane wave density functional theory. A broad peak (or three predominant modes) was observed consistently in theory (278.9 cm^{-1}, 282.0 cm^{-1}, 283.0 cm^{-1}) and experiment. These three modes demonstrate the structural flexibilities in the hexagonal pore-breathing mechanisms along directions roughly parallel to *c*, *a*, *b* crystal directions, respectively, with almost equal intensities. Illustrations of these modes can be found in the Supporting Information.

A time trace of MOF growth tracked by MIR spectroscopy is shown in Figure 5B. The spectra are very similar to that observed in the literature for Co-MOF 74 and are reproduced solvent-free as the black curve in the

figure. Also shown is the theoretical calculation marked in red. Exact frequencies can be found in the Supporting Information. We have chosen to work with a set of peaks collected in the FIR and MIR region to track the growth kinetics as a function of temperature. Figure S3 shows the kinetics traces for MOF synthesis 60 °C measured by FIR and MIR at 239, 580, 1196, and 1480 cm^{-1}, along with their corresponding errors measured from three sets of data.

Figure S4 shows the time dependence of the Co-MOF-74 reaction by tracking the peaks at 239 and 580 cm^{-1} (FIR) and 1196, 1408, and 1556 cm^{-1} (MIR) over 60 min at 55, 60, 65, and 70 °C. The 239 cm^{-1} peak arises from the structural flexibilities in the hexagonal pore-breathing mode, the 580 cm^{-1} peak is from Co-O stretching, 1196 cm^{-1} is from in-plane C-H bending, 1408 cm^{-1} is from aromatic C-C stretching and finally the C=O stretching is at 1556 cm^{-1}. These modes are also shown in the Table S1. The results broadly follow those observed from the Raman and WAXS data from the capillary measurements, slow growth up to around 60 °C and then a very sharp rise as the temperature is ramped to 65 °C, the onset of reaction is around 2 min, compared to 10 min at 60 °C and 20 min at 55 °C. However, there are slight differences between the FIR and MIR rise curves, particularly for the 65 °C dataset, where, while the onset is similar, the rise is much more rapid in the MIR range. This could possibly mean that the lattice takes a somewhat longer time to form as the reaction accelerates with an increase in temperature.

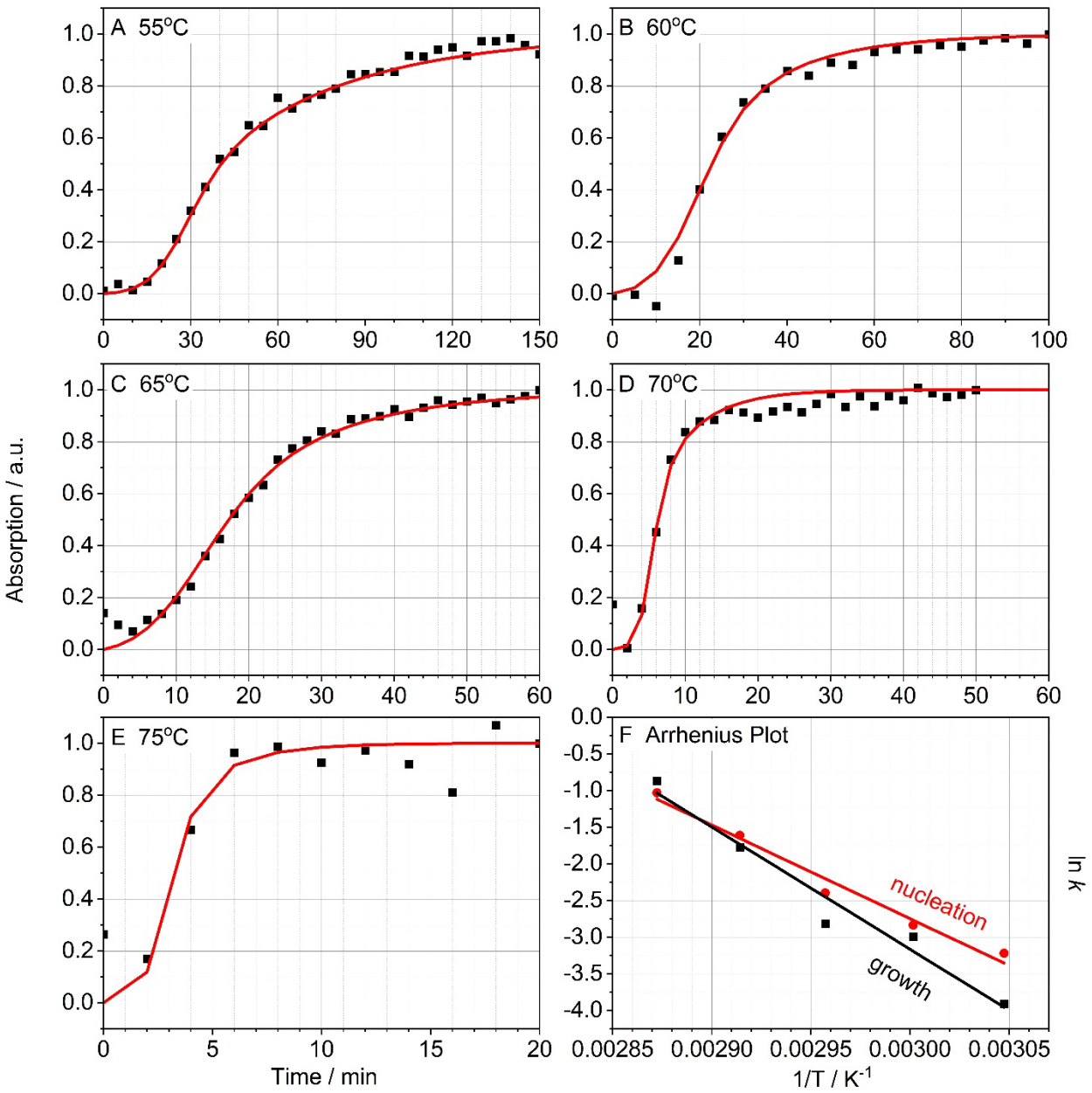

Figure 6 Gualtieri model fitting (red curves) for the reaction kinetics traced by absorption intensity of 580 cm^{-1} (black symbols) as a function of time at temperatures of (A) 55 °C, (B) 60 °C, (C) 65 °C, (D) 70 °C, (E) 75 °C. (F) Arrhenius Plots for nucleation (red) and growth (black) extracted from rate constants derived from the fitted parameters shown in (A) – (E).

Earlier studies of Co-MOF-74 growth[16] used a mathematical model, developed by Gualtieri to parameterize zeolite growth kinetics,[33] to simulate crystallization and separate the nucleation and growth rate constants. This method has also recently been applied to probe MOF (MFM-500(Ni)) growth using NMR spectroscopy.[34]

$$I = 1 - \left\{\left(1 - \exp(-(k_g t)^n)\right)/(1 + \exp(-(t - k_n^{-1})b^{-1}))\right\}$$

Here *I* correspond to the Intensity of the 580 cm^{-1} peak, k_g and k_n are rates of growth and nucleation, *n* denotes the dimensionality of the growth (*n* = 1, 2, or 3 for one-, two-, or three-dimensional growth, respectively) and *b* is proportional to the standard deviation of the mean nucleation time (essentially the inverse of the nucleation rate constant). We fit our 580 cm^{-1} peak from the FIR spectra to this model and the results are shown in Figure 6 for temperatures of 55, 60, 65, 70, and 75 °C. The model allowed us to generate the rate constant for crystal growth (k_g) and nucleation (k_n). From these rates, we generated Arrhenius parameters, shown in Figure 6F. We extract activation energies of 102.0 kJ/mol for nucleation and 138.7 kJ/mol growth. This can be compared with the bulk growth kinetics measured by Osta et al.[16], who measured 66.5 and 90.4 kJ/mol for nucleation and growth respectively. In Figure S4, we superimposed their growth curves measured using X-ray diffraction at 70 and 80 °C to our 580 cm^{-1} curves measured at 65 and 70 °C respectively. It is interesting that we are extracting reasonable reaction kinetics information for MOF synthesis using only 1 µmol H_4dobdc and 3.5 µmol of cobalt acetate solution for the synthesis of Co-MOF-74 on the ATR chip, compared to the traditional synthesis that uses 0.5 mmol of H_4DHTP and 0.5 mmol of metal nitrate hexahydrate in sealed reaction vessels.

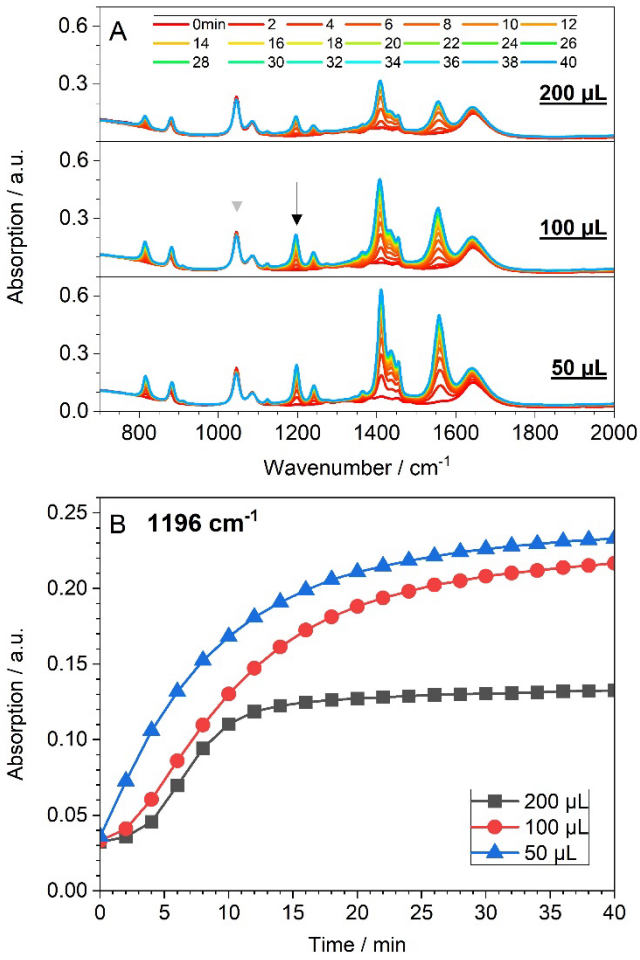

Figure 7 (A) MIR spectra recorded at 65 °C reactor temperature for a reagent volume of 200, 100 and 50 µL in the ATR reservoir. The arrows indicate reagent and MOF peaks discussed in the text. (B) Time traces for the 1196 cm^{-1} vibrational mode at 200, 100 and 50 µL reagent volume.

Our reactor geometry and ability to discern chemical signatures from microscopic volumes in a controlled manner lends itself to the exploration of "active matter",[35] a topic of interest in the broader chemical synthesis community. Experimental reports[36] have emerged where molecular mobility has been claimed to be "boosted" in chemical reactions. Furthermore, the role of solvent[37, 38] (water) and confinement,[39] to accelerate and catalyze chemical reactions has also been discussed both experimentally[40] and theoretically[41] in the literature. As is evident from the MOF crystals formed in this work compared to those in the literature, it would appear that volume can play an active role in synthesis. An exploratory experiment where the volume of reagents was varied from 50 to 100 to 200 µL showed that the kinetics traces recorded at 1196 cm^{-1} did change (Figure 7). The rate of reaction increased as the volume was lowered. We hypothesize that this is due to the availability of reactants to reach the surface of the ATR chip more rapidly when the volume is decreased. Since heterogeneous nucleation occurs at sites on surfaces, plus the effect of gravity, the ATR chip on the bottom served as a nucleation site that immediately detected the newly formed Co-MOF-74 crystals. We also observed that the MOF was mostly well deposited on the ATR chip whereas the solution remained clear after the reaction. This might be a significant contribution to the accelerated 'apparent reaction rate'. The internal diameter of the O-ring that holds the reactor to the ATR chip is 7 mm, which translated to a surface area of 38.5 mm^2. The ATR geometry used will typically allow for the IR to be sensitive to around 1 – 10 µm in the wavelength region of 400 – 4000 cm^{-1}. The peak at 1047 cm^{-1} is from the ethanol/water solvent, and can act as a marker for the rate of enhancement for MOF formation, by comparing its intensity to that of the 1196 cm^{-1} peak. While there is barely any drop in its intensity for each volume and time, the rates of MOF formation change dramatically across both these parameters. On the other hand, a larger volume covers a larger surface area including the inner wall of the reactor and the ATR chip, with only the MOF deposited on the ATR chip (bottom) being detectable. Therefore, a larger volume would have more MOF formed on the inner wall of the reactor, being unable to detect.

In our experiment, the reagents were introduced via a micropipette, in the future, active control of reagent concentration will be performed using microfluidics. We envision digital control of temperature, reagent concentration and volume to actively control and drive MOF formation and growth. An added advantage of these microliter volumes is that it becomes reasonably easy to vary the reaction parameters and probe the resultant kinetics using table top spectroscopy instruments. A recent *in-situ* microfluidic set up to probe MOF thin film growth used mmol/L flowrates using similar Si based wafers as the internal reflection element on a customized ATR-FTIR instrument.[42] In those experiments, atomic layer deposition was used to deposit a nucleation layer onto the surface. Adjusting the flow rate, let to different reaction rates. Our experimental strategy lends itself to incorporation of such microfluidic flow approaches, but with vastly reduced volume of material, while the open nature of the top will allow inclusion of other multimodal tools to probe MOF nucleation and growth.

Our theory provides a molecular-level understanding of the reaction dynamics and further corroborates the experimental findings, suggesting that future experiments on gas uptake and dynamics measurements will be able to provide both molecular and structural information simultaneously. At present, our Raman measurements are sensitive to around 150 cm^{-1}, future upgrades should allow us to access the THz region. Typically, THz, Raman, and FIR spectroscopy has been used to probe gas uptake and dynamics of already formed MOFs. Our capillary and chip-based methods allow for a MOF to be synthesized on the fly and processed (in situ activation of the MOF) for gas uptake measurements, while simultaneously using the

extended vibrational region available with our spectrometers to probe synthesis and dynamics within a single experiment.

Our multiscale tools applied to probing MOF nucleation and growth are readily applicable to guide and understand chemical transformations in diverse contexts[43] such as molecular self-assembly,[44] and heterogeneous processes in confined spaces.[45] These transformations are described by complex free energy landscapes that determine correlated atomic and molecular motions over multiple length and time scales. More exact and explicit descriptions of the molecular interactions and predictions of their direct experimental observables are to be pursued, with the goal of informing an increasingly realistic and highly dimensional "digital twin" that aims to explain experiments by mirroring the physical world. Such a "digital twin"[43, 46] approach, recently employed in understanding photoelectron spectroscopy measurements[47] will target the incorporation of active control of reaction parameters coupled to precise experimental spectroscopic observables in analyzing the resulting data sets through iterative theory-experiment feedback loops. This will allow a hypothesis-driven tool kit to be added to understanding the complex chemical pathways that can lead to molecular growth and ultimately materials nucleation and growth.

Conflicts of interest

There are no conflicts to declare.

Acknowledgements

MA, WL, EZ, and CW are supported by the Director, Office of Science, Office of Basic Energy Sciences, of the U.S. Department of Energy under Contract No. DE-AC02-05CH11231, through the Condensed Phase, Interfaces and Molecular Sciences Program, Chemical Sciences Division. JQ is supported by the Director, Office of Science, Office of Basic Energy Sciences, of the U.S. Department of Energy under Contract No. DE-AC02-05CH11231 through the Gas Phase Chemical Physics Program. The Advanced Light Source and CZ are supported by the same contract. The contributions of MNJ and JRL were supported by the U.S. Department of Energy Office of Basic Energy Sciences under award DE-SC0019992. We are further grateful for the support of MNJ through an Arnold O. Beckman Postdoctoral Fellowship.

References

1. X. Chen, H. Gao, Z. Tang and G. Wang, *Cell Rep. Phys. Sci.*, 2020, **1**.
2. L. Feng, K.-Y. Wang, J. Powell and H.-C. Zhou, *Matter*, 2019, **1**, 801-824.
3. T. M. McDonald, J. A. Mason, X. Kong, E. D. Bloch, D. Gygi, A. Dani, V. Crocellà, F. Giordanino, S. O. Odoh, W. S. Drisdell, B. Vlaisavljevich, A. L. Dzubak, R. Poloni, S. K. Schnell, N. Planas, K. Lee, T. Pascal, L. F. Wan, D. Prendergast, J. B. Neaton, B. Smit, J. B. Kortright, L. Gagliardi, S. Bordiga, J. A. Reimer and J. R. Long, *Nature*, 2015, **519**, 303-308.
4. J. E. Bachman, Z. P. Smith, T. Li, T. Xu and J. R. Long, *Nat. Mater.*, 2016, **15**, 845-849.
5. Y. Zheng, S. Zheng, H. Xue and H. Pang, *J. Mater. Chem. A*, 2019, **7**, 3469-3491.
6. D. J. Xiao, E. D. Bloch, J. A. Mason, W. L. Queen, M. R. Hudson, N. Planas, J. Borycz, A. L. Dzubak, P. Verma, K. Lee, F. Bonino, V. Crocellà, J. Yano, S. Bordiga, D. G. Truhlar, L. Gagliardi, C. M. Brown and J. R. Long, *Nat. Chem.*, 2014, **6**, 590-595.
7. C.-Y. Sun, C. Qin, X.-L. Wang and Z.-M. Su, *Expert Opin. Drug Deliv.*, 2013, **10**, 89-101.
8. H. Furukawa, K. E. Cordova, M. O'Keeffe and O. M. Yaghi, *Science*, 2013, **341**, 1230444.
9. M. J. Van Vleet, T. Weng, X. Li and J. R. Schmidt, *Chem. Rev.*, 2018, **118**, 3681-3721.

10. L. Hanna and J. V. Lockard, *J. Phys. Condens. Matter*, 2019, **31**, 483001.
11. H. H. Yeung, Y. Wu, S. Henke, A. K. Cheetham, D. O'Hare and R. I. Walton, *Angew. Chem. Int. Ed. Engl.*, 2016, **55**, 2012-2016.
12. X. Liu, S. W. Chee, S. Raj, M. Sawczyk, P. Kral and U. Mirsaidov, *Proc. Natl. Acad. Sci. U.S.A.*, 2021, **118**.
13. L. Kollias, R. Rousseau, V. A. Glezakou and M. Salvalaglio, *J. Am. Chem. Soc.*, 2022, **144**, 11099-11109.
14. E. Haque and S. H. Jhung, *Chem. Eng. J.*, 2011, **173**, 866-872.
15. E. Roh, I. Subiyanto, W. Choi, Y. C. Park, C.-H. Cho and H. Kim, *Bull. Kor. Chem. Soc.*, 2021, **42**, 459-462.
16. R. El Osta, M. Feyand, N. Stock, F. Millange and R. I. Walton, *Powder Diffr.*, 2013, **28**, S256-S275.
17. J. Beamish-Cook, K. Shankland, C. A. Murray and P. Vaqueiro, *Cryst. Growth Des.*, 2021, **21**, 3047-3055.
18. J. D. Evans, V. Bon, I. Senkovska, H. C. Lee and S. Kaskel, *Nat. Commun.*, 2020, **11**, 2690.
19. D. J. Cerasale, D. C. Ward and T. L. Easun, *Nat. Rev. Chem.*, 2021, DOI: 10.1038/s41570-021-00336-8.
20. X. Li, C. Yang, B. Sun, S. Cai, Z. Chen, Y. Lv, J. Zhang and Y. Liu, *J. Mater. Chem. A*, 2020, **8**, 16045-16060.
21. Z. Liu, J. Zhu, T. Wakihara and T. Okubo, *Inorg. Chem. Front.*, 2019, **6**, 14-31.
22. J. D. Smith, C. D. Cappa, W. S. Drisdell, R. C. Cohen and R. J. Saykally, *J. Am. Chem. Soc.*, 2006, **128**, 12892-12898.
23. C. Weeraratna, C. Amarasinghe, W. Lu and M. Ahmed, *J. Phys. Chem. Lett.*, 2021, **12**, 5503-5511.
24. J. P. Perdew, K. Burke and M. Ernzerhof, *Phys. Rev.Lett.*, 1996, **77**, 3865-3868.
25. G. Kresse and D. Joubert, *Phys. Rev. B.*, 1999, **59**, 1758-1775.
26. B. Vlaisavljevich, J. Huck, Z. Hulvey, K. Lee, J. A. Mason, J. B. Neaton, J. R. Long, C. M. Brown, D. Alfè, A. Michaelides and B. Smit, *J. Phys. Chem. A*, 2017, **121**, 4139-4151.
27. K. Lee, J. D. Howe, L.-C. Lin, B. Smit and J. B. Neaton, *Chem. Mater.*, 2015, **27**, 668-678.
28. S. Baroni, S. de Gironcoli, A. Dal Corso and P. Giannozzi, *Rev. Mod. Phys.*, 2001, **73**, 515-562.
29. K. Refson, P. R. Tulip and S. J. Clark, *Phys. Rev. B.*, 2006, **73**, 155114.
30. A. Togo and I. Tanaka, *Scr. Mater.*, 2015, **108**, 1-5.
31. N. L. Rosi, J. Kim, M. Eddaoudi, B. Chen, M. O'Keeffe and O. M. Yaghi, *J. Am. Chem. Soc.*, 2005, **127**, 1504-1518.
32. P. D. Dietzel, P. A. Georgiev, J. Eckert, R. Blom, T. Strassle and T. Unruh, *Chem. Commun.*, 2010, **46**, 4962-4964.
33. A. F. Gualtieri, *Phys. Chem. Miner.*, 2001, **28**, 719-728.
34. C. L. Jones, C. E. Hughes, H. H. Yeung, A. Paul, K. D. M. Harris and T. L. Easun, *Chem. Sci.*, 2020, **12**, 1486-1494.
35. C. Bechinger, R. Di Leonardo, H. Löwen, C. Reichhardt, G. Volpe and G. Volpe, *Rev. Mod. Phys.*, 2016, **88**.
36. H. Wang, M. Park, R. Dong, J. Kim, Y. K. Cho, T. Tlusty and S. Granick, *Science*, 2020, **369**, 537-541.
37. T. Kitanosono and S. Kobayashi, *Chem.*, 2020, **26**, 9408-9429.
38. G. Li, B. Wang and D. E. Resasco, *ACS Catal.*, 2019, **10**, 1294-1309.
39. Z. Wei, Y. Li, R. G. Cooks and X. Yan, *Annu. Rev. Phys. Chem.*, 2020, **71**, 31-51.
40. G. Rovelli, M. I. Jacobs, M. D. Willis, R. J. Rapf, A. M. Prophet and K. R. Wilson, *Chem. Sci.*, 2020, **11**, 13026-13043.
41. L. R. Pestana, H. Hao and T. Head-Gordon, *Nano Lett.*, 2020, **20**, 606-611.

42. J. Zhao, B. Kalanyan, H. F. Barton, B. A. Sperling and G. N. Parsons, *Chem. Mater.*, 2017, **29**, 8804-8810.
43. M. Ahmed, M. Blum, E. J. Crumlin, P. L. Geissler, T. Head-Gordon, D. T. Limmer, K. K. Mandadapu, R. J. Saykally and K. R. Wilson, *J. Phys. Chem. B*, 2021, **125**, 9037-9051.
44. D. Biswal and P. G. Kusalik, *ACS Nano*, 2017, **11**, 258-268.
45. F. C. Meldrum and C. O'Shaughnessy, *Adv. Mater.*, 2020, **32**, e2001068.
46. J. Qian and E. Crumlin, presented in part at the Proceedings of 7th Annual Ambient Pressure XPS Workshop, Pohang, Korea, Dec 15−17, 2020., 2021.
47. J. Qian, A. Baskin, Z. Liu, D. Prendergast and E. J. Crumlin, *J. Chem. Phys.*, 2020, **153**, 044709.